Full Paper

Propellants, Explosives, Pyrotechnics

DOI: 10.1002/prep.201900376

Embedded Manganin Gauge Measurements and Modeling of Shock Initiation in HMX-Based PBX Explosives with Different Particle Sizes and Porosities

Zhiling Bai,[a] Zhuoping Duan,*[a] Lijing Wen,[b] Zhenyu Zhang,[c] Zhuocheng Ou,[a] and Fenglei Huang[a]

Abstract: A series of shock initiation experiments on the explosive PBXC03 (87% HMX, 7% TATB, and 6% Viton by weight) with different particle sizes and porosities under various shock loadings have been performed, and it is found that the particle size and the porosity of the explosives have much influence on the shock initiation characteristics. That is, the smaller the particle size, the more difficult the explosive to be ignited but the faster the detonation grows once the explosive is ignited. It is also found that the detonation grows the fastest in the explosive with moderate porosity. Moreover, a modified mesoscopic reaction rate model based on the experimental results and the pore collapse hot-spot ignition mechanism is developed, which allows for a separate reaction mechanism evaluation at different reaction stages for the shock initiation and detonation growth processes in the explosives. The calculated pressure-time histories and Pop-Plots for PBXC03 are founded to be all in good agreement with the experimental data. The modified mesoscopic reaction rate model shows its potentiality for quantitatively predicting the effects of the mesostructure of PBXs on the shock initiation and detonation growth processes with a high degree of confidence.

Keywords: Shock initiation · Lagrangian experimental system · Modified mesoscopic reaction rate model · Particle size · Porosity · PBX explosive

1 Introduction

Polymer bonded explosives (PBXs), one kind of the pressed heterogeneous solid explosives that composed of the main explosive grains (such as RDX, HMX, PETN, TATB, etc.) or their mixtures and a few percent of polymer binders, together with a small amount of porosity, have attracted much academic attention due to their high energy and insensitive properties, which has also stimulated the synthesis of insensitive high composite explosives [1–3]. Investigations into the initiation mechanisms and the ignition and detonation growth behaviors of a heterogeneous solid explosive under the external shock-wave loadings have been a critical issue in practical military and/or civil engineering applications for a long time [4, 5], in which a core problem is to choose an available reactive flow model for the explosives, including the calibration of the model parameters, to quantitatively and accurately predict the shock initiation and subsequent detonation processes in the explosives.

It has been suggested that the pore collapse (e.g., the viscoplastic deformation, the hydrodynamic micro jetting, the compression of gas in cavities and the shear bandings) is a dominant hot-spot generation mechanism for the shock initiation in pressed solid explosives [6–10]. Numerous researches have investigated the pore collapse hot-spot ignition mechanism via experiments (the voids in mm-scale) [11–13], molecular dynamics (MD) simulations [14, 15] and mesoscale simulations [16, 17], suggesting that the initial size and shape of the pore, the material viscosity, and the shock pressure have noticeable effects on the hot spot formation. These studies have permitted a closer micro-mechanical description and accurate prediction of the pore collapse hot spot formation mechanisms. However, it is worth mentioning here that few attempts have been made to bridge the gap between the micro/mesoscale simulations and the macro-scale experimental measurements. The main challenge for their works lies in developing a reactive flow model with an explicit mathematical expression to describe the actual complicated pore collapse processes. For instance, as the pore pinches shut, that the upstream materials may penetrate into the downstream pore wall under the high pressure. However, it is difficult to obtain the

[a] *Z. Bai, Z. Duan, Z. Ou, F. Huang*
The State Key Laboratory of Explosion Science and Technology, Beijing Institute of Technology, Beijing 100081, China
**e-mail: duanzp@bit.edu.cn*
[b] *L. Wen*
Nuclear and Radiation Safety Center, Ministry of Environmental Protection, Beijing 100082, China
[c] *Z. Zhang*
Institute of Technical Physics, College of Science, National University of Defense Technology, Changsha 410073, China

mathematical characterization for the actual complicated asymmetric collapse processes and the corresponding hot-spot ignition reaction rate. To overcome this limitation and develop a chemical reaction rate model with a simply explicit mathematical expression to describe the important features dominating the pore collapse processes, the void collapse is usually assumed to be spherically symmetric [18, 19], which allows for the one-dimensional deformation with an analytical solution of the governing equations and an explicit expression of the chemical reaction rate for the convenience of industrial application. For a realistic size explosive charge, to some extent, the above-simplified approach is reasonable for over thousands of individual hot spot dimensions. Recently, a double-layers hollow sphere model (the DZK model) to describe the shock initiation behaviors of PBXs has been proposed by Duan et al. [20], in which a low-pressure slow reaction [18] and high-pressure fast reaction terms [21] are introduced to describe the detonation growth process. The DZK model is used to describe the influence of the initial temperature, the shock loading and the mesostructure characteristics (e.g., the particle size, porosity, binder's content and strength) on the ignition and the detonation growth processes of PBXs [20, 22]. Up to now, the DZK model is generally accepted due to the advantage that, compared with the most commonly used Ignition and Growth model developed by Lee and Tarver [23, 24], fewer parameters in the DZK model need to be determined. However, further studies show that the typical pressure increasing rate calculated using the DZK model is usually faster than the experimental data [22]. Moreover, this model fails to estimate the influence of the explosive density (or porosity) on the shock initiation characteristics, which is just the motivation of modifying the DZK model in this study.

On the other hand, it is believed that the mesostructure of a heterogeneous solid explosive has a significant influence on its shock initiation characteristics [8, 25], which has not yet been thoroughly understood. The experimental measurements have provided enormous insight into the understanding of shock initiation and detonation growth processes in the explosives. However, in fact, to date, most of the previous research on the shock initiation of PBXs focused mainly on the macro-scale effects, such as that of the loading pressure [26], the initial temperature [27–31] and damage of the explosive [32], but to the influence of the mesoscale morphology of the explosive particles have not yet been paid much attention. For example, the particle size, one of the important parameters of the particle morphology, determines directly the initial number of the potential hot-spots and the average size of these sites and hence must play a more and more important role in describing the ignition and the detonation growth processes of PBXs.

The present work, therefore, aims at investigating experimentally and numerically the influence of the particle size and the porosity of PBXC03 (87% HMX, 7% TATB, and 6% Viton by weight) as well as that of the shock loadings on the ignition and the detonation growth processes. A modified mesoscopic reaction rate model (the modified DZK model) is then developed, together with the introduction of a burn-up and a porosity factors into the DZK model to describe effects of the outer burning on the surfaces of explosive grains at the low-pressure slow reactive stage and the initial charge density, respectively. This paper is divided into five major sections as follows. After this brief introduction, the experimental set-up is described in Section 2. In Section 3, the modified DZK reactive rate model is developed, and the ignition and the detonation growth processes are simulated numerically based on the modified DZK model in Section 4, together with the comparison between the numerical results and the experimental data. Finally, in Section 5, some conclusions are drawn out.

2 Experimental Set-Up

A one-dimensional Lagrangian experimental system for shock initiation is adopted to measure the pressure-time histories at different Lagrangian locations of PBXC03 (87% HMX, 7% TATB, and 6% Viton by weight) with different particle sizes and porosities under various shock loadings ($P_0 =$ 4.5, 5.2 and 5.9 GPa). The experimental set-up is shown in Figure 1, in which, an explosive plane-wave lens with a diameter of 60 mm and a TNT booster of 60 mm in diameter and 20 mm in height are used to generate a high-pressure planar detonation wave loading. The thickness of the aluminum clapboard is 13 mm, and different shock-wave loadings can be obtained directly by adjusting the thickness of the air-gap ring. Moreover, a multilayer PBXC03 sample of 50 mm in diameter consists of three thin discs (3, 4 or 5 mm, respectively) and a thick piece in a thickness of 25 mm. Four H-type manganin gauges were embedded between adjacent discs to measure the in-situ pressure-time histories. Additionally, to prolong the pressure-measuring time, the manganin gauges are coated with the Teflon insulation sheets, and the thicknesses of the Teflon insulation sheets used for the first and the last three gauges are 0.2 mm and 0.1 mm, respectively.

The electric resistance R_0 of the manganin piezoresistive pressure gauge is $0.1 \sim 0.2\ \Omega$, and the pressure-resistance relation is [33]:

$$P = (0.76356 \pm 0.1811) + (34.62796 \pm 0.96071)\left(\frac{\Delta R}{R_0}\right) + (6.00762 \pm 0.97841)\left(\frac{\Delta R}{R_0}\right)^2 \quad (1)$$

where P is the pressure (GPa), R_0 and ΔR are the electric resistance and its increment, respectively, of the gauge; $\Delta R/R_0 = \Delta U/U_0$, where U_0 and ΔU are the corresponding voltage and its increment of the voltage across the gauge recorded

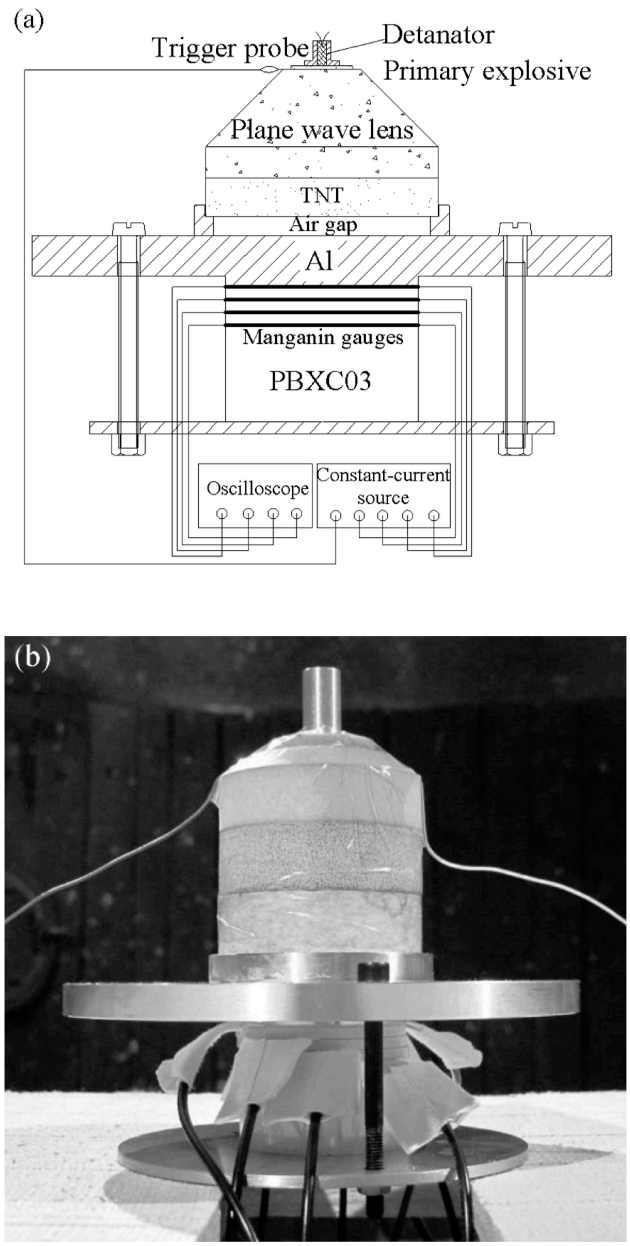

Figure 1. One-dimensional Lagrangian experimental system for shock initiation. (a) Schematic diagram of the experimental set-up; (b) Photograph of a typical shock initiation experiment driven by the explosive detonation.

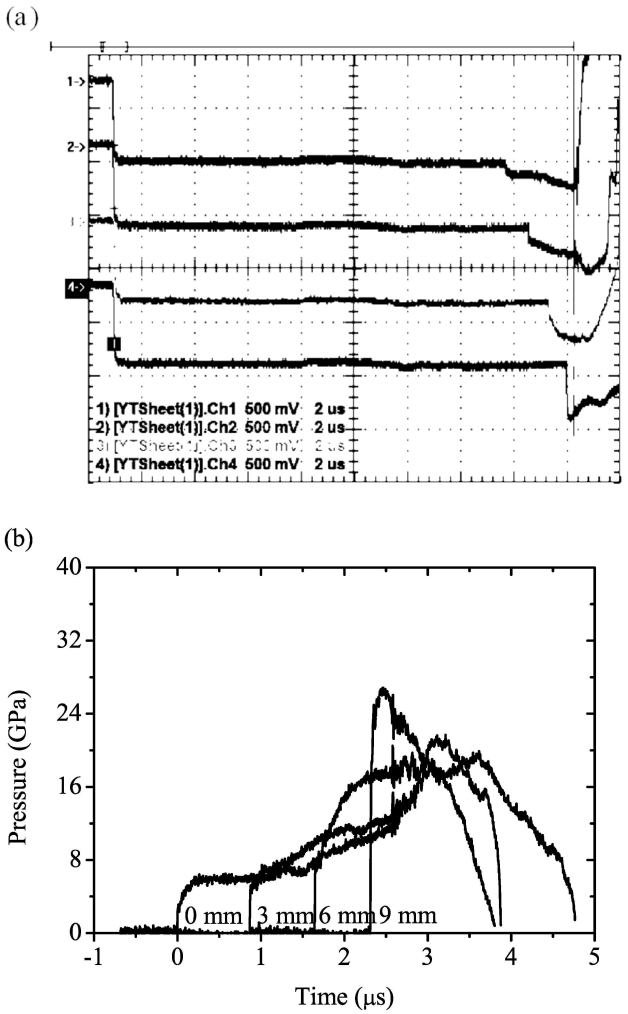

Figure 2. A typical experimental data. (a) Voltage signals recorded by the oscilloscope; (b) Pressure histories in the PBXC03 explosive.

by the oscilloscope, respectively. The typical measured voltage signals and the converted pressure-time histories obtained from Eq. (1) are shown in Figure 2, where the Arabic numerals on the lower right corner of each curve represent the Lagrange distances from the initial impacting surface of the explosive sample.

A series of PBXC03 samples with different densities (or porosities) and particle sizes are designed and used in the experiments. The detailed components proportion and the physical parameters of the used PBXC03 explosives are listed in Table 1. To facilitate the comparison with the numerical results, all the experimental data are presented in Section 4.

To verify the repeatability of the experimental data, the pressure-time curves at 0 mm in different experiments (see Figure 4 and Figure 7 in Section 4, respectively) under the

Table 1. The components proportion and the physical parameters of the PBXC03 explosive.

Components proportion HMX/TATB/Viton	Density (g/cm^3)	Mean particle size (μm) HMX	TATB
87/7/6 (by weight)	1.836	20 ~ 30 (fine particle)	15
85.58/6.76/7.66 (by volume)	1.849	70 ~ 90 (medium particle)	
	1.855	110 ~ 130 (coarse particle)	

same initial loading pressure of 5.9 GPa are compared, as shown in Figure 3. It can be seen that these curves almost overlap completely at the platform stage, which implies that the loading conditions are consistent and the testing system is stable and reliable (The pressure growth rates at the later stage are different with various formula of the explosive samples).

3 The Modified DZK Reaction Rate Model

The DZK reaction rate model proposed by Duan et al. [20] is:

$$\frac{\mathrm{d}\lambda}{\mathrm{d}t} = \frac{\mathrm{d}\lambda_{\text{ignition}}}{\mathrm{d}t} + \frac{3\lambda^{2/3}}{r_\mathrm{o}} a p^n + G p^m (1-\lambda)^s \tag{2}$$

where the subscript "ignition" denotes the hot-spot ignition contribution, and λ is the overall reaction degree (the volume fraction of the reacted explosive) at the time t; p is the current pressure, r_o is the average radius of the explosive particles, and a, n, G, m, and s are constant coefficients. Moreover, the first term on the right-hand side of Eq. (2) describes the hot-spot forming phase, and the last two terms describe the slow-burning at the low-pressure stage and the fast reaction at the high-pressure phase, respectively.

Assume that there are enough hot spots in the explosive, and the hot spot around a pore is similar to all other hot spots in the vicinity and, therefore, a representative double-layered hollow sphere collapse hot-spot model can be used to study the hot-spot ignition characteristic of explosives. Duan et al. [20] deduced the collapse velocity and the temperature distribution over the spherical cell, and then the hot-spot ignition term can be expressions as follows:

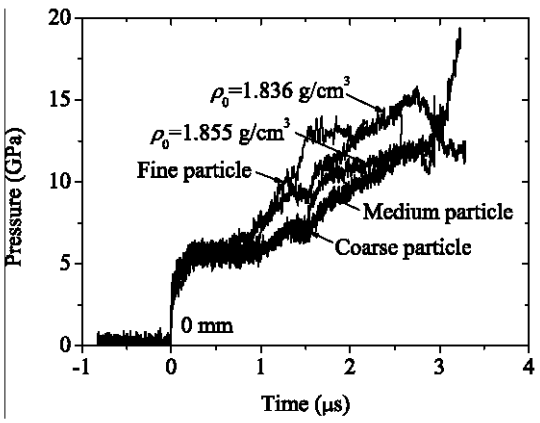

Figure 3. Comparison among the pressure-time curves at 0 mm in different experiments under the same loading pressure.

$$\frac{\mathrm{d}\lambda_{\text{ignition}}}{\mathrm{d}t} = \int_{r_\mathrm{i}}^{r_\mathrm{o}} \frac{\frac{\mathrm{d}\Lambda}{\mathrm{d}t}(r,t) 4\pi r^2}{\frac{4}{3}\pi\left(r_\mathrm{o}^3 - r_\mathrm{i}^3\right)} \mathrm{d}r \tag{3}$$

$$\frac{\mathrm{d}\Lambda(r,t)}{\mathrm{d}t} = (1-\Lambda) Z \exp\left(-\frac{T^*}{T(r,t)}\right) \tag{4}$$

$$T = T_0(r,t) + \int_0^t \frac{\mathrm{d}T}{\mathrm{d}t}(r,t)\mathrm{d}t \tag{5}$$

$$\frac{\mathrm{d}T}{\mathrm{d}t} = \left(\frac{\mathrm{d}T}{\mathrm{d}t}\right)_{\text{M.D.}} + \frac{1}{\rho C_p}\frac{1}{r^2}\left(r^2 k^* \frac{\partial T}{\partial r}\right) + \frac{Q}{\rho C_p}\frac{\mathrm{d}\Lambda(r,t)}{\mathrm{d}t} \tag{6}$$

$$\left(\frac{\mathrm{d}T}{\mathrm{d}t}\right)_{\text{M.D.}} = \left(\frac{3\gamma_\mathrm{e}\gamma_\mathrm{b}^2 k_\mathrm{e}}{2\rho C_p}\right) \times \frac{\left(P_0 - P_g - 2\sqrt{3}k_\mathrm{b}\ln\frac{r_\mathrm{m}}{r_\mathrm{i}} - 2\sqrt{3}k_\mathrm{e}\ln\frac{r_\mathrm{o}}{r_\mathrm{m}}\right)^2}{\left[\left(r_\mathrm{o}^{-3} - r_\mathrm{m}^{-3}\right)\gamma_\mathrm{b}k_\mathrm{e} + \left(r_\mathrm{m}^{-3} - r_\mathrm{i}^{-3}\right)\gamma_\mathrm{e}k_\mathrm{b}\right]^2 r^6} \tag{7}$$

where $\Lambda(r, t)$ is the local reaction degree; Z is the pre-exponential factor in Arrhenius kinetics; T^*, T_0, and T are the activation temperature, the initial temperature, and the current temperature, respectively; k^*, C_p and Q are the thermal conductivity, the heat capacity and the reaction heat of the explosive, respectively. Moreover, subscripts "M.D.", "e" and "b" denote the mechanical deformation, the explosive and the binder, respectively. $\gamma_{\mathrm{e,b}} = (\gamma_1\sigma_0)_{\mathrm{e,b}}$ and $k_{\mathrm{e,b}} = \sigma_{0\mathrm{e,b}}/\sqrt{3}$, where γ_1 is a constant coefficient, and σ_0, k are the static and the shear yield strength, respectively.

It suggests that the DZK reaction rate model can be used to describe the influence of the initial temperature, the particle size and the porosity of the explosive, the binder's strength and content, and the loading pressure on the shock ignition and the detonation growth processes of heterogeneous solid explosives [20, 22]. However, the typical pressure-time curves calculated by using the DZK model don't agree so well with the experimental data. For example, the experimental data show that the pressure increasing rate goes through a slow-fast-slow process until the maximum pressure, while, in contrast, the pressure increasing rates calculated by using the DZK model increase monotonously until the maximum pressure. In the opinion of the present authors, this is because that the low-pressure slow-burning term in the DZK model involved only the internal pore combustion, and, as the reaction proceeds, the combustion surface area increases rapidly, which leads to a swiftly increase of the gas products pressure until the completion of the reaction. In fact, the explosive reaction is a process of multi-hot-spots combustion, and the combustion topology contains both the internal pore and the outer particle surface combustion modes. During the combustion process, the inner pore surface area increases and the outer explosive particle surface area decreases. Therefore, the total combustion surface area increases slowly at the low-pressure slow reaction stage, and hence the pressure in-

creases slowly. To overcome such a difficulty in the DZK model, in this paper, a burn-up factor $(1-\lambda)^b$ is introduced to describe the outer particle surface combustion in the low-pressure slow reaction term, where b is a constant coefficient. Furthermore, refer to the Ignition and Growth model [23, 24], a porosity factor $1-|1-\rho_0/\rho_T-c|^y$ is further introduced, where both c and y are constant coefficients. Finally, the modified DZK reaction rate model is proposed, as:

$$\frac{d\lambda}{dt}=\frac{d\lambda_{ignition}}{dt}+\frac{3\lambda^{2/3}(1-\lambda)^b}{r_o}ap^n\left[1-\left|1-\frac{\rho_0}{\rho_T}-c\right|^y\right]+Gp^m(1-\lambda)^s \quad (8)$$

where the parameters in the first hot-spot ignition term (Eqs. (3)–(7)) are the thermodynamic parameters of explosives itself [20] and that in the last two combustion terms are determined by fitting a typical experimental data, as listed in Table 2, which are also used in the following numerical simulations in section 4.

Moreover, Eq. (8) can then be integrated to give

$$\lambda=\lambda_{ignition}+\lambda_{slow}+\lambda_{fast} \quad (9)$$

where $\lambda_{ignition}$, λ_{slow}, and λ_{fast} represent the contributions of the hot-spot ignition term, the low-pressure slow combustion term, and the high-pressure fast reaction term, respectively. Eq.(9) allows for a separate reaction mechanism evaluation at different reaction stages for the shock initiation and detonation growth processes in the explosives.

In addition, the Jones-Wilkins-Lee (JWL) equations of state (EOS) are adopted for the detonation products and the unreacted explosive, and both are in the following temperature-dependent form:

$$p=Ae^{-R_1\bar{V}}+Be^{-R_2\bar{V}}+\frac{\omega C_v}{\bar{V}}T \quad (10)$$

where $\bar{V}$ p and T are current pressure, relative volume and temperature, respectively, A, B, R_1, R_2, ω, and C_v are constant coefficients. The values of the parameters in Eq. (10) for PBXC03 with different densities are listed in Table 3 and Table 4, respectively. It should be pointed out here that the detonation performance of the explosive (such as the detonation velocity and the detonation pressure) depends on its density. The parameters R_1, R_2 and ω can be assumed as constants under small change of the charge density, and the parameters A, B and C are determined according to the compatibility relations [34].

4 Results and Discussion

The modified DZK reaction rate model is incorporated into a hydrocode DYNA2D to simulate numerically the shock ignition and the detonation growth processes of PBXC03, in which the sub-grid technology is adopted to implement the pore collapse hot-spot process. Moreover, a variable-density aluminum flyer plate impact model is adopted, and the manganin gauges and the Teflon films are also embedded in the explosive model.

The isotropic-elastoplastic-hydrodynamic material constitutive model is adopted for PBXC03, in which the corresponding modeling parameters include the initial density ρ_0, the shear modulus $G\tau=0.0352$ Mbar and the yield strength $k_Y=0.0020$ Mbar. Moreover, the Grüeneisen equations of state for the aluminum flyer plate, the manganin pressure gauge and the Teflon film in the following form are used:

Table 2. Parameters of the modified DZK reaction rate model for the PBXC03 explosive at room temperature.

Hot-spot ignition term [20]		Second and third terms (this work)	
$Z(\mu s^{-1})$	5.0e13	a	0.017
T^* (K)	26500	b	1.86
T_0 (K)	298	n	0.965
C_p ($cm^2/\mu s^2/K$)	1.4e–5	c	0.0128
$Q(cm^2/\mu s^2)$	5.439e–2	y	0.125
k^* (cm/μs/K)	8.0e–14	G	590.0
k_e (Mbar)	8.0e–5	m	3.195
γ_e (μs^{-1})	0.026	s	1.00

Table 3. Parameters of the JWL EOS for the detonation products of PBXC03 with different densities at room temperature.

Parameters	$\rho_0=1.836$ g/cm^3 (This work)	$\rho_0=1.849$ g/cm^3 [34]	$\rho_0=1.855$ g/cm^3 (This work)
A (Mbar)	10.027	10.254	10.314
B (Mbar)	0.229	0.226	0.235
R_1	4.91	4.91	4.91
R_2	1.37	1.37	1.37
ω	0.29	0.29	0.29
C_v (Mbar/K)	1.0E-5	1.0E-5	1.0E-5
E_0 (Mbar)	0.096	0.096	0.096

Table 4. Parameters of the JWL EOS for the unreacted PBXC03 explosive with different densities at room temperature.

Parameters	$\rho_0=1.836$ g/cm^3 (This work)	$\rho_0=1.849$ g/cm^3 [34]	$\rho_0=1.855$ g/cm^3 (This work)
A(Mbar)	2.655E5	2.721E5	2.775E5
B(Mbar)	−0.734	−0.739	−0.739
R_1	19.87	19.87	19.87
R_2	1.987	1.987	1.987
ω	1.99	1.99	1.99
C_v(Mbar/K)	1.687E-4	1.693E-4	1.698E-4

$$p = \frac{\rho_0 C^2 \mu \left[1 + \left(1 - \frac{\gamma_0}{2}\right)\mu - \frac{a}{2}\mu^2\right]}{\left[1 + (S_1 - 1)\mu - S_2 \frac{\mu^2}{1+\mu} - S_3 \frac{\mu^3}{(1+\mu)^2}\right]^2} + (\gamma_0 + a\mu)E \qquad (11)$$

where p is the current pressure; ρ_0 is the initial density; C is the intercept of the shock wave velocity-particle velocity curve; S_1, S_2, and S_3 are slope coefficients of the particle velocity curve, respectively; γ_0 is the Grüeneisen coefficient; a is the first-order volume correction factor; E is the specific internal energy, and $\mu = \rho/\rho_0 - 1$ the compressibility factor. The values of the parameters in the equations of state are listed in Table 5 [35].

The numerical results for the pressure histories and the pressure growth processes on the precursory shock wavefront in the PBXC03 explosive with different particle sizes and porosities under various loading pressures, together with the corresponding experimental data, are shown in Figure 4–Figure 11, respectively. It can be seen that the numerical results are all in good agreement with the experimental data, which indicates that the modified DZK reaction rate model can preferably predict the influence of the particle size and the porosity of explosives and the shock loadings on the shock initiation processes of PBXs.

As shown in Figure 4, under the same peak loading pressure $P_0 = 5.9$ GPa, the PBXC03 explosives of fine particle size with three different porosities (or densities) are used to investigate the influence of the porosity on the ignition and the detonation growth processes. Figure 5 shows the pressure-increasing processes on the precursory shock wavefront in PBXC03. It can be clearly seen that the detonation grows the fastest in the explosive with a moderate density under the loading and the charge conditions in this paper. To make further analysis of the specific reason, the degree of chemical reaction-time histories in the reaction flow field are printed out, as shown in Figure 6, wherein (a)-(d) are the time histories of the overall reaction degree λ, the contributions of the hot-spot ignition term $\lambda_{ignition}$, the low-pressure slow combustion term λ_{slow} and the high-pressure fast reaction term λ_{fast}, respectively. It is found that the hot-spot ignition reacts the fastest in the explosive with a low density (see Figure 6(b)) because the mean size of the potential hot spots in the explosive with a high porosity are largest, and hence there are most reactive hot spots, which results in the fastest energy release and hence the hot-spot ignition reacts fastest. However, the optimal combustion topology (with the maximum burning surface area) can be achieved in the explosive with a moderate density due to the modest compression when it was charged, which makes the combustion reaction fastest in the explosive with a moderate density at the low-pressure slow combustion stage (see Figure 6(c)). In other words, the shock initiation of a heterogeneous explosive is dominated mainly by the

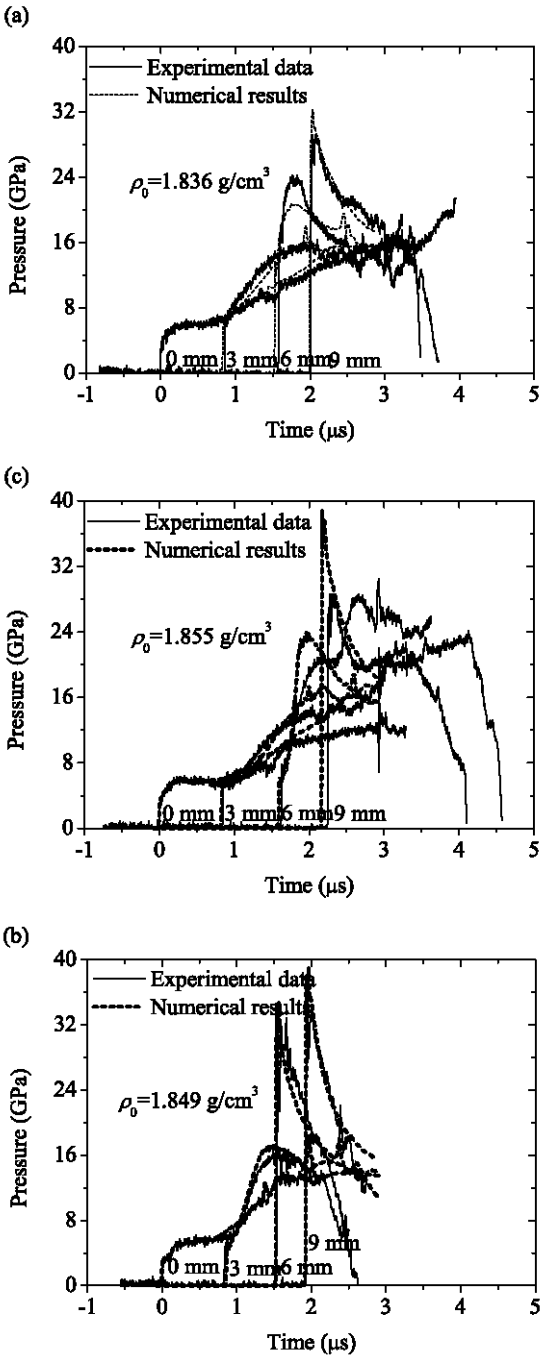

Figure 4. Experimental data and Numerical results for the pressure histories in PBXC03 with different porosities (or densities): (a) $\rho_0 =$ 1.836 g/cm^3, (b) $\rho_0 = 1.849$ g/cm^3, (c) $\rho_0 = 1.855$ g/cm^3.

Table 5. Parameters in the Grüeneisen equations of state [35].

Materials	ρ_0 (g/cm^3)	C (cm/μs)	S_1	S_2	S_3	γ_0	a
Al	2.705 ~ 2.785	0.524	1.4	0	0	1.97	0.48
Manganin	8.14	0.394	1.489	0	0	2.02	0.47
Teflon	2.15	0.168	1.123	3.983	−5.797	0.59	0

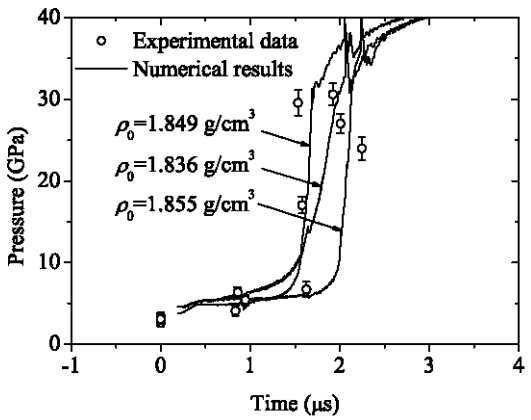

Figure 5. Experimental data and Numerical results for the pressure growth on the precursory shock wavefront in PBXC03 with different porosities (or densities).

hot-spot ignition and the combustion processes, and the mesostructure of the heterogeneous explosive has different effects on the mechanical reaction at different reaction stages. Certainly, the influence of the porosities on the ignition and detonation processes of PBXs is also dependent on the loading pressure. For instance, under a higher loading pressure, the combustion reaction plays a dominant role in the ignition and detonation processes, which may slow down monotonically with the decrease of the porosity.

It is worth noting here that the calculated time history of the degree of hot-spot ignition $\lambda_{ignition}$ in Figure 6(b) is a non-smooth curve (exhibit a shape of step increasing) and this is related to the sub-grid technology used in the hot-spot ignition term (Eqs. (3)–(7)) of the modified DZK model. The curve will be much smoother with the increasing spatial mesh steps, and which is chosen to be 10 in this work to improve the computational efficiency while maintaining the solution accuracy. Moreover, at the early stage of pore collapse, the local temperature is relatively low, which makes the hot-spot ignition reaction exceedingly slow until about 0.25 μs (~0.43 μs) that the hot-spot ignition reaction becomes faster, as shown in Figure 6(b). The value of 0.25 μs (or 0.43 μs) can be approximately regarded as the so-called induction time for ignition.

Under the same peak loading pressure $P_0 = 5.9$ GPa, the PBXC03 explosives with the medium density $\rho_0 = 1.849$ g/cm^3 and three different particle sizes are used to investigate the influence of the explosive's particle size on the shock initiation characteristics (see Figure 7). As shown in Figure 8, for the explosive with smaller particle size, the precursory shock wave pressure increases slowly in the earlier phase but faster at the later stage, while, on the contrary, for the coarse particle explosive, there is a relatively large pressure-increasing at the earlier stage but slowly at a later stage. These results can be better explained from the point of view that the mesostructure of the heterogeneous ex-

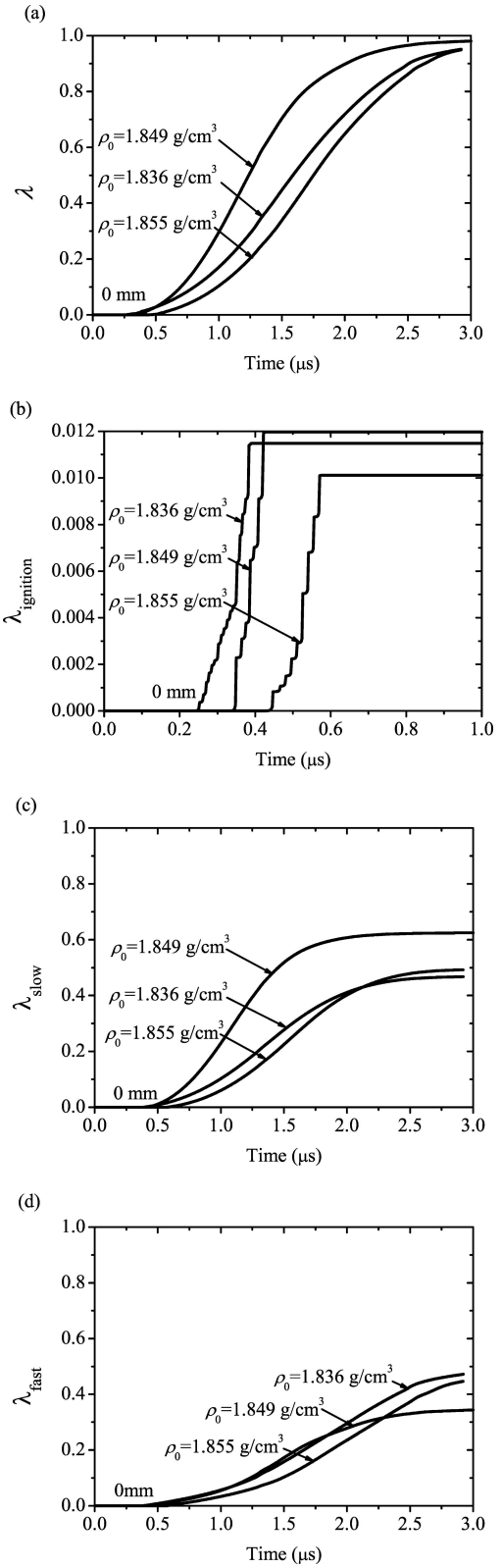

Figure 6. Degree of chemical reaction-time curves in PBXC03 with different porosities: time histories of (a) λ, (b) $\lambda_{ignition}$, (c) λ_{slow}, and (d) λ_{fast}.

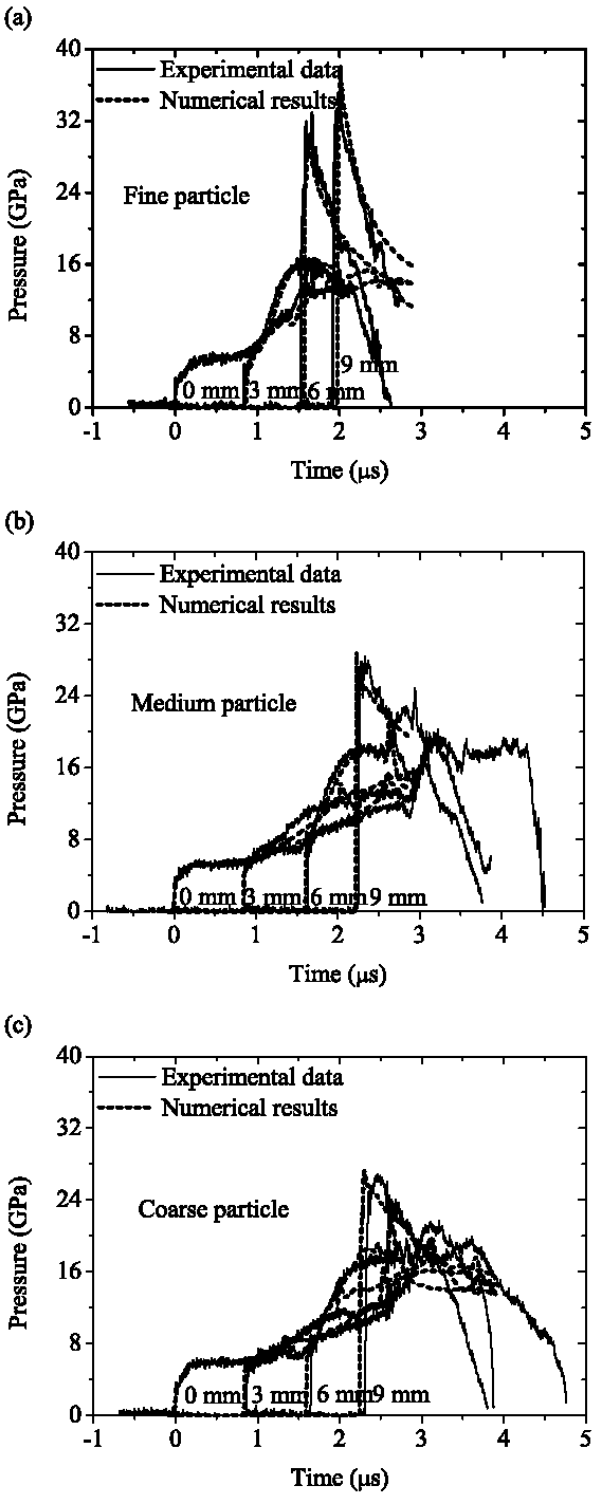

Figure 7. Experimental data and Numerical results for the pressure histories in the PBXC03 explosives with different particle sizes: (a) the fine particle, (b) the medium particle and (c) the coarse particle.

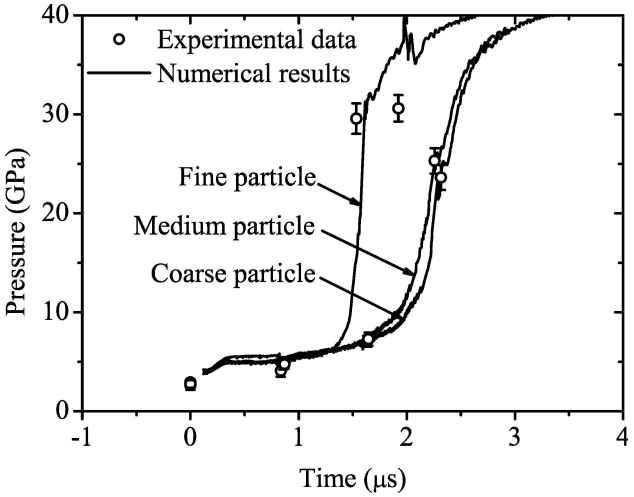

Figure 8. Experimental data and Numerical results for the pressure growth on precursory shock wavefront in the PBXC03 explosives with different particle sizes.

plosive at different reaction stages has different effects on the mechanical reaction as shown in Figure 9. The size of the potential hot spots is smaller in the explosive with smaller particle size, and hence there are relatively fewer reactive hot spots and the hot-spot ignition reaction is slower in the explosive (see Figure 9(b)), which results in a slower energy release and hence the hot-spot ignition has little contribution to the precursory shock wave. However, once the explosive with smaller particle size has been ignited, the faster reaction occurs due to the larger combustion surface (see Figure 9(c)), and the pressure increases more quickly too, which leads to the shorter run distance and time to detonation. On the other hand, for the coarse particle explosive, the sizes of potential hot-spots are relatively larger, and a large number of reactive hot spots release energy quickly, which directly promotes the precursory shock wave pressure. After the hot-spots ignite, the combustion reaction is slower because of the smaller combustion surface, and the pressure increases more slowly. In other words, under the loading and the charge conditions in this paper, the smaller the particle size of the explosive, the more difficult the explosive to be ignited but the faster the detonation growth once the explosive has been ignited.

In addition, it should be pointed out here that the influence of the particle size on the shock initiation will depend on the loading pressure. For example, under a lower loading pressure, the hot-spot ignition plays a dominant role in the shock initiation, which may slow down with the decrease of the particle size, while, under a higher loading pressure, the number of the reactive hot-spots reaches saturation, and thus the shock initiation is dominated by the combustion process, which becomes fast with the decrease of the particle size.

The PBXC03 explosives with coarse particle size and the medium density $\rho_0 = 1.849$ g/cm^3 are used in this study to investigate the effects of the shock-wave loadings on the

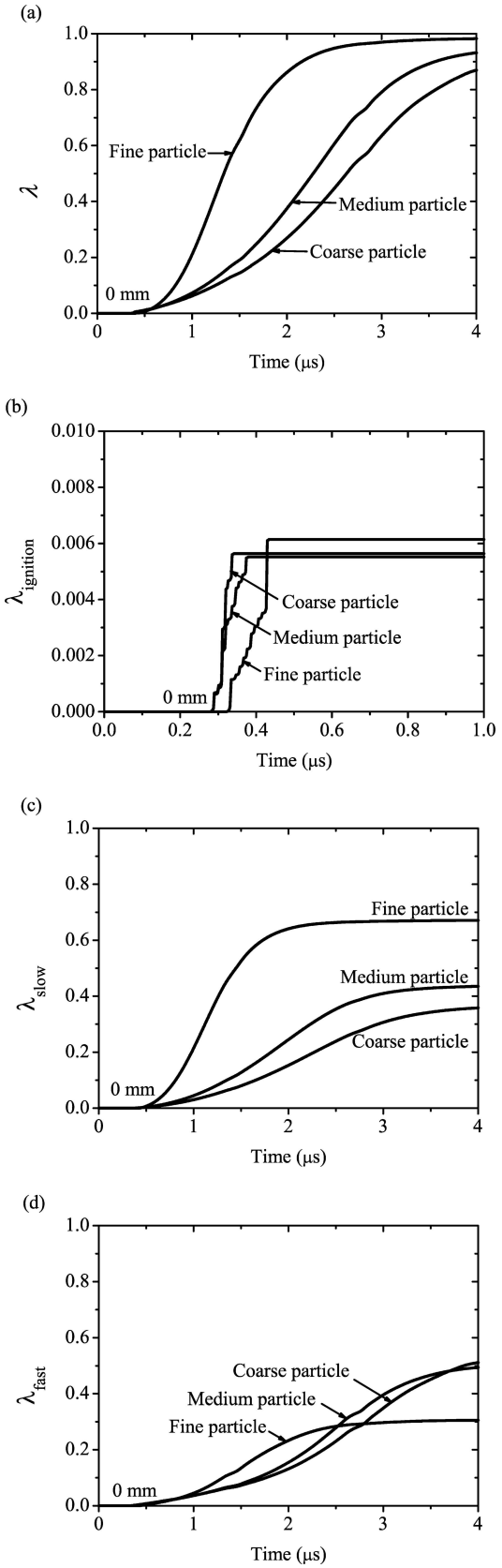

Figure 9. Degree of chemical reaction-time curves in PBXC03 with different particle sizes: time histories of (a) λ, (b) $\lambda_{ignition}$, (c) λ_{slow}, and (d) λ_{fast}.

ignition and the detonation growth processes, as shown in Figure 10. Figure 11 shows the pressure growth processes on the precursory shock wavefront in PBXC03, it can be clearly seen that the higher the loading pressure, the faster the precursory shock wave pressure grows, and the shorter the run distance to detonation. From the physical point of view, the higher the pressure, the higher the temperature of the potential hot-spots and the smaller the critical size of the reactive hot-spots [25,36]. That is, with the increase of the initial shock loading, there are more reactive hot-spots in the explosive, which makes both the hot-spots ignite and the combustion reacts more quickly, as shown in Figure 12.

Figure 13 shows the calculated "Pop-Plots" for PBXC03 with three different particle sizes (the charge density $\rho_0 =$ 1.849 g/cm^3) by using the modified DZK model, together with the comparison between this work and previous experimental data. The symbol "☆" represents the measurement results by using the multiple electromagnetic particle velocity gauge [37], and the solid line shows the Pop-Plot for PBXC03 in the reference of the Laboratory Manual of Explosives [38], i.e.,

$$\log(P_0) = (1.03 \pm 0.04) - (0.48 \pm 0.04)\log(L) \quad (2.35\ \text{GPa} < P_0 < 8.03\ \text{GPa}) \tag{12}$$

where P_0 is the loading pressure (GPa), and L is the run distance to detonation (mm). The dark grey area in Figure 13 is the range of the allowable error shown in Eq. (12). It can be seen that the calculated Pop-Plots by the modified DZK model are basically in good agreement with the previous experimental data.

The whole process of shock initiation to stable detonation calculated by the modified DZK model is shown in Figure 14, in which the dash line shows the pressure growth process on the precursory shock wavefront (where the degree of reaction $\lambda = 0$) and the Von Neumann peak pressure P_N for stable detonation is on this curve. Moreover, the dotted line indicates the pressure state at the end of the reaction zone ($\lambda = 1$). It is worth mentioning here that, in theory, the CJ (Chapman-Jouguet) state should fall on this curve, but the calculated pressure at the end of the reaction zone is usually lower than the detonation pressure P_{CJ}, which is related to the artificial viscous force used in the numerical calculation. Because when dealing with the problem of singularity of strong shock wave by using the artificial viscous force, the shock wavefront is "widened" for several grids, which results in the delay of the calculated time of the end of reaction zone ($\lambda = 1$), and hence the obtained pressure at the end of reaction zone is lower than the detonation pressure P_{CJ}. In this paper, the calculated Von Neumann peak pressure P_N is 46 GPa, and the detonation pressure P_{CJ} is 35.6 GPa. The duration of the chemical reaction zone from the precursory shock wavefront to the CJ state is 110 ns, and the width of the reaction zone is 0.59 mm. These calculated results are in good agreement with previously published experimental results [39,40]. Compared

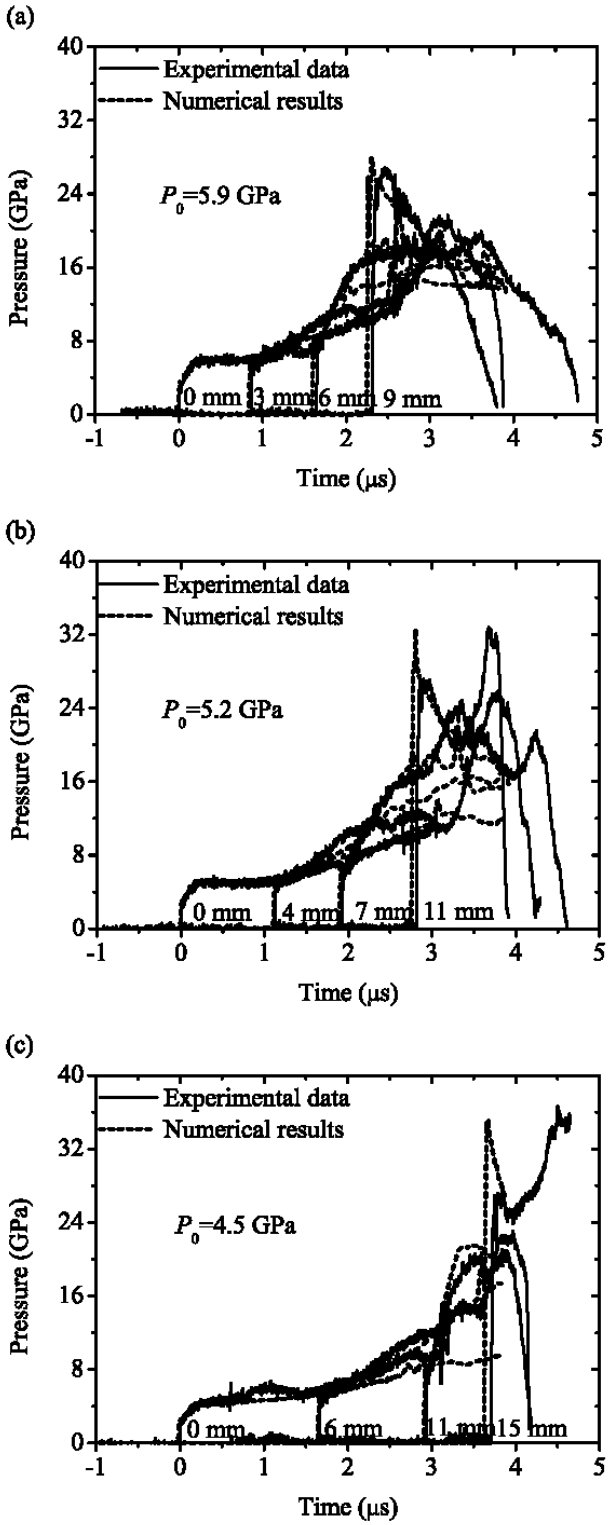

Figure 10. Experimental data and Numerical results for the pressure histories in PBXC03 under different loading pressures: (a) P_0= 5.9 GPa, (b) P_0=5.2 GPa, (c) P_0=4.5 GPa.

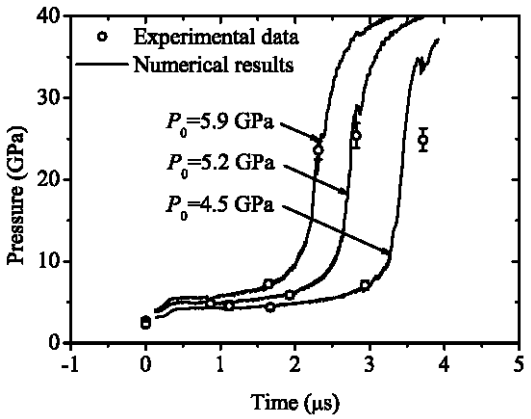

Figure 11. Experimental data and Numerical results for the pressure growth on the precursory shock wavefront in PBXC03 under different loading pressures.

with the most commonly used Ignition and Growth model, the modified DZK reaction rate model with one set of parameters shows its potentiality for preferably describing both the shock initiation process and the stable detonation process in the PBX explosive with a high degree of confidence.

5 Conclusions

Shock initiation experiments on the explosive PBXC03 were performed to obtain in-situ pressure gauge data for investigating the influence of the particle size, the porosity and the shock loadings on the shock initiation and subsequent detonation growth processes of PBXs. It is found that the detonation grows the fastest in the explosive with a moderate porosity, and the smaller the explosive's particle size, the more difficult the explosive to be ignited but faster the detonation grows once the explosive has been ignited. Based on experiments and numerical simulations, a modified DZK reaction rate model is proposed by introducing a burn-up and porosity factors to describe the effects of the outer burning on the surfaces of explosive grains at the low-pressure slow reactive stage and the initial charge density, respectively. This model can predict well the influence of the particle size, the porosity and the shock loadings on the shock initiation (i.e., ignition and detonation growth) processes of PBXs, and the calculated pressure-time histories and Pop-Plots are in good agreement with the experimental data. Compared with the most commonly used Ignition and Growth model, the modified DZK reaction rate model with one set of parameters shows its potentiality for preferably describing both the shock initiation process and the stable detonation process in the PBX explosive with a high degree of confidence.

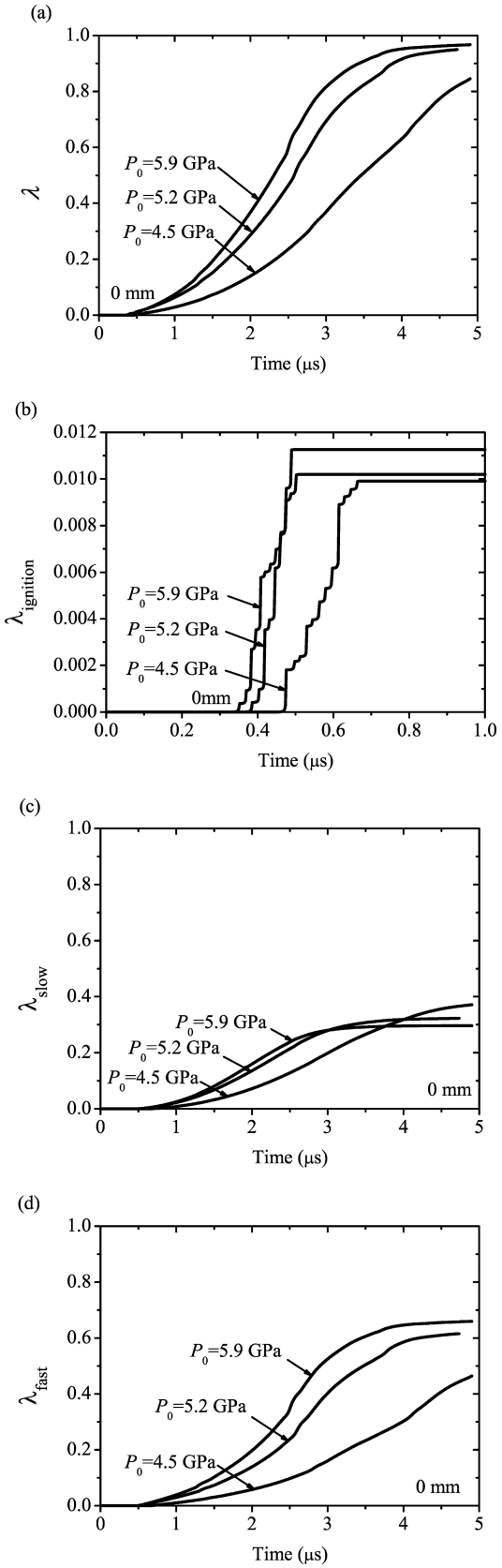

Figure 12. Degree of chemical reaction-time curves in PBXC03 under different loading pressures: time histories of (a) λ, (b) $\lambda_{ignition}$, (c) λ_{slow}, and (d) λ_{fast}.

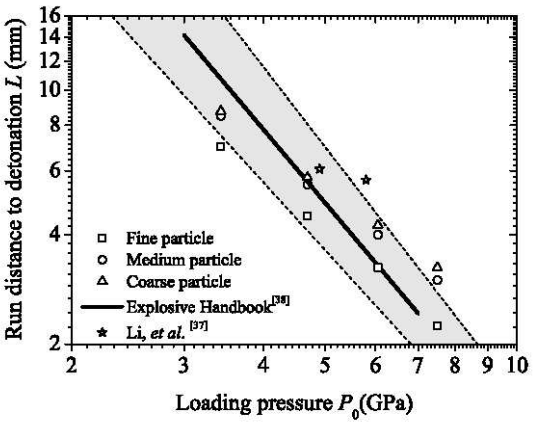

Figure 13. Pop-Plots for PBXC03 with different particle sizes and comparison of the data from this work with that of previous experiments.

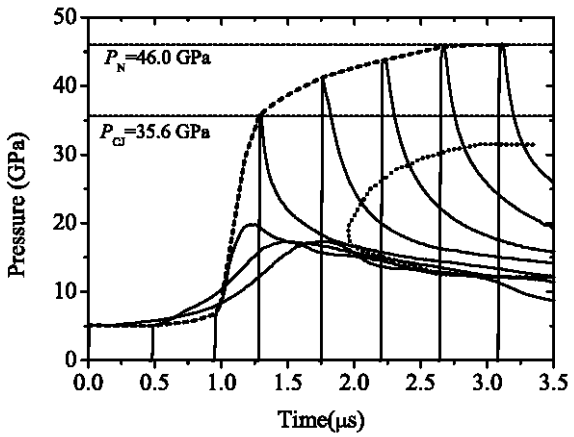

Figure 14. The calculated shock initiation and detonation growth processes in PBXC03

Acknowledgments

This work was supported by the NSAF Joint Fund Jointly set up by the National Natural Science Foundation of China and the China Academy of Engineering Physics (Grants No. U1630113) and the Innovative Group of Material and Structure Impact Dynamics (Grants No. 11521062). The experiments were done in Institute of Chemical Materials, China Academy of Engineering Physics, and thanks for providing great support for the experiments.

References

[1] C. An, H. Li, B. Ye, C. Xu, J. Wang, Preparation and Characterization of Ultrafine HMX/TATB Explosive Co-Crystals, *Cent. Eur. J. Energ. Mater.* **2017**, *14*, 876–887.

[2] M. B. Talawar, A. P. Agarwal, M. Anniyappan, G. M. Gore, S. N. Asthana, S. Venugopalan, Method for Preparation of Fine TATB

(2-5 μm) and its Evaluation in Plastic Bonded Explosive (PBX) Formulations, *J. Hazard. Mater.* **2006**, *137*, 1848.

[3] Z. Wang, X. Guo, F. Wu, T. Yan, Preparation of HMX/TATB Composite Particles Using a Mechanochemical Approach, *Propellants Explos. Pyrotech.* **2016**, *41*, 327–333.

[4] A. Becuwe, A. Delclos, Low-Sensitivity Explosive Compounds for Low Vulnerability Warheads, *Propellants Explos. Pyrotech.* **1993**, *18*, 1–10.

[5] K. Elsharkawy, G. Lin, H. Fouda, Experimental Studies on Improved Plastic Bonded Explosives Materials (PBXs) for Controlled Fragmentation Warheads, *MATEC. Web Conf.* **2017**, *88*, 03001.

[6] R. B. Frey, Cavity Collapse in Energetic Materials, *8th Symposium (International) on Detonation,* Albuquerque, NM, USA, July 15 – 19, **1985**, pp. 68–80.

[7] A. Kapahi, H. S. Udaykumar, Dynamics of Void Collapse in Shocked Energetic Materials: Physics of Void–Void Interactions, *Combust. Explos. Shock Waves* **2013**, *23*, 537–558.

[8] J. Massoni, R. Saurel, G. Baudin, G. Demol, A Mechanistic Model for Shock Initiation of Solid Explosives, *Phys. Fluids.* **1999**, *11*, 710–736.

[9] L. Tran, H. S. Udaykumar, Simulation of Void Collapse in an Energetic Material, Part 1: Inert Case, *J. Propul. Power.* **2006**, *22*, 947–958.

[10] L. Tran, H. S. Udaykumar, Simulation of Void Collapse in an Energetic Material, Part 2: Reactive Case, *J. Propul. Power.* **2006**, *22*, 959–974.

[11] N. K. Bourne, On the Collapse of Cavities, *Combust. Explos. Shock Waves* **2002**, *11*, 447–455.

[12] N. K. Bourne, A. M. Milne, The Temperature of a Shock-Collapsed Cavity, *Proc. R. Soc. London, Ser. A,* **2003**, *459*, 1851–1861.

[13] A. B. Swantek, J. M. Austin, Collapse of Void Arrays under Stress Wave Loading, *J. Fluid Mech.* **2010**, *649*, 399–427.

[14] T. Zhou, J. Lou, Y. Zhang, H. Song, F. Huang, Hot Spot Formation and Chemical Reaction Initiation in Shocked HMX Crystals with Nanovoids: a Large-Scale Reactive Molecular Dynamics Study, *Phys. Chem. Chem. Phys.* **2016**, *18*, 17627–17645.

[15] R. M. Eason, T. D. Sewell, Molecular Dynamics Simulations of the Collapse of a Cylindrical Pore in the Energetic Material α-RDX, *J. Dynamic Behavior Mater.* **2015**, *1*, 423–438.

[16] A. Kapahi, H. S. Udaykumar, Three-Dimensional Simulations of Dynamics of Void Collapse in Energetic Materials, *Combust. Explos. Shock Waves* **2015**, *25*, 177–187.

[17] N. K. Rai, M. J. Schmidt, H. S. Udaykumar, High-Resolution Simulations of Cylindrical Void Collapse in Energetic Materials: Effect of Primary and Secondary Collapse on Initiation Thresholds, *Phys. Rev.* **2017**, 2.

[18] K. Kim, Development of a Model of Reaction Rates in Shocked Multicomponent Explosives, *9th Symposium (International) on Detonation*, Portland, OR, USA, August 28 – September 1, **1989**, pp. 593–603.

[19] K. Kim, C. H. Sohn, Modeling of Reaction Buildup Processes in Shocked Porous Explosives, *8th Symposium (International) on Detonation,* Albuquerque, NM, USA, July 15 – 19, **1985**, pp. 926–933.

[20] Z. P. Duan, L. J. Wen, Y. Liu, Z. C. Ou, F. L. Huang, Z. Y. Zhang, A Pore Collapse Model for Hot-Spot Ignition in Shocked Multi-Component Explosives, *Int. J. Nonlin. Sci. Num. Simul.* **2010**, *11*, 19–24.

[21] Z. D. Tian, Z. Y. Zhang, A Mesomechanic Model of Shock Initiation in PBX-9404 Explosive, *Chin. J. Energet. Mater.* **2007**, *15*, 464–467.

[22] L. J. Wen, Z. P. Duan, L. S. Zhang, Z. Y. Zhang, Z. C. Ou, F. L. Huang, Effects of HMX Particle Size on the Shock Initiation of PBXC03 Explosive, *Int. J. Nonlin. Sci. Num. Simul.* **2012**, *13*, 189–194.

[23] E. L. Lee, C. M. Tarver, Phenomenological Model of Shock Initiation in Heterogeneous Explosives, *Phys. Fluids* **1980**, *23*, 2362–2372.

[24] C. M. Tarver, J. O. Hallquist, L. M. Erickson, Modeling Short Pulse Duration Shock Initiation of Solid Explosives, *8th Symposium (International) on Detonation,* Albuquerque, NM, USA, July 15 – 19, **1985**, pp. 951–961.

[25] K. F. Grebenkin, Comparative Analysis of Physical Mechanisms of Detonation Initiation in HMX and in a Low-Sensitive Explosive (TATB), *Combust. Explos. Shock Waves* **2009**, *45*, 78–87.

[26] J. W. Forbes, C. M. Tarver, G. Urtiew, F. Garcia, The Effects of Confinement and Temperature on the Shock Sensitivity of Solid Explosives, *11th Symposium (International) on Detonation,* Snowmass Village, CO, USA, August 31 – September 4, **1998**, pp. 145–152 .

[27] R. L. Gustavsen, S. A. Sheffield, R. R. Alcon, J. W. Forbes, C. M. Tarver, F. Garcia, Embedded Electromagnetic Gauge Measurements and Modeling of Shock Initiation in the TATB Based Explosives LX-17 and PBX 9502, *12th Conference of the American Physical Society Topical Group on Shock Compression of Condensed Matter,* Atlanta, Georgia (USA), June 24 – 29, **2001**, AIP Conference Proceedings 620, p.p 1019–1022.

[28] R. N. Mulford, R. R. Alcon, Shock Initiation of PBX-9502 at Elevated Temperatures, *9th Conference of the American Physical Society Topical Group on Shock Compression of Condensed Matter,* Seattle, Washington (USA), August 13 – 18, **1995**, AIP Conference Proceedings 370, p. 855, DOI: https://doi.org/10.1063/1.50582.

[29] S. A. Sheffield, R. L. Gustavsen, L. G. Hill, R. R. Alcon, Electromagnetic Gauge Measurements of Shock Initiating PBX9501 and PBX9502 Explosives, *11th Symposium (International) on Detonation,* Snowmass Village, CO, USA, August 31 – September 4, **1998**, pp. 451–458.

[30] P. A. Urtiew, C. M. Tarver, J. W. Forbes, F. Garcia, Shock Sensitivity of LX-04 at Elevated Temperatures, *10th Conference of the American Physical Society Topical Group on Shock Compression of Condensed Matter,* Amherst, Massachusetts (USA), July 27 – August 1, **1997**, AIP Conference Proceedings 429, pp., 727–730.

[31] K. S. Vandersall, C. M. Tarver, F. Garcia, P. A. Urtiew, Shock Initiation Experiments on PBX9501 Explosive at 150 °C for Ignition and Growth Modeling. *14th Conference of the American Physical Society Topical Group on Shock Compression of Condensed Matter*, Baltimore, Maryland (USA), July 31 – August 5, **2005**, AIP Conference proceedings 845, pp., 1127–1130.

[32] S. K. Chidester, K. S. Vandersall, C. M. Tarver, Shock Initiation of Damaged Explosives, *JANNAF Interagency Propulsion Committee*, Tucson, AZ, Lawrence Livermore National Laboratory, **2009**.

[33] Z. P. Duan, Y. Liu, A. G. Pi, F. L. Huang, Foil-Like Manganin Gauges for Dynamic High Pressure Measurements, *Meas. Sci. Technol.* **2011**, *22*, 075206.

[34] L. J. Wen, *Research on Mesoscopic Reaction Rate Model of Shock Initiation of PBX*, Beijing Institute of Technology, Beijing, **2011**.

[35] P. A. Urtiew, K. S. Vandersall, C. M. Tarver, F. Garcia, *Initiation of Heated PBX-9501 Explosive When Exposed to Dynamic Loading*, Report UCRL-CONF-214667, Lawrence Livermore National Laboratory, Livermore, CA (United States), **2005**.

[36] C. M. Tarver, S. K. C. And, A. L. N. Iii, Critical Conditions for Impact- and Shock-Induced Hot Spots in Solid Explosives†, *J. Phys. Chem.* **1996**, *100*, 5794–5799.

[37] Z. P. Li, X. P. Long, Y. M. Huang, B. He, R. Wang, S. W. He, Study and Application of the Multiple Electromagnetic Particle Velocity Gauge Technique, *Energ. Mater.*, **2005**, *13*, 359–361 (in Chinese).

[38] H. S. Dong, F. F. Zhou, *Performance of High Energetic Explosive and Related Compound*, Science Press, Beijing, **1989** (in Chinese).

[39] J. N. Fritz, R. S. Hixson, M. S. Shaw, C. E. Morris, R. G. McQueen, Overdriven-Detonation and Sound-Speed Measurements in PBX-9501 and the "Thermodynamic" Chapman-Jouguet Pressure, *J. Appl. Phys.* **1996**, *80*, 6129–6141.

[40] A. V. Fedorov, A. L. Mikhailov, L. K. Antonyuk, D. V. Nazarov, S. A. Finyushin, Determination of Chemical Reaction Zone Parameters, Neumann Peak Parameters, and the State in the Chapman-Jouguet Plane in Homogeneous and Heterogeneous High Explosives, *Combust. Explos. Shock Waves* **2012**, *48*, 302–308.

Manuscript received: November 7, 2019
Revised manuscript received: November 19, 2019
Version of record online: March 10, 2020

